Supporting information

T.S. Sukhikh[a,b*], D.S. Kolybalov[a,b], E.K. Pylova[a,b], D.A. Bashirov[a,b], V.Y. Komarov[a,b], N.V. Kuratieva[a,b], A.I. Smolentsev[a], A.N. Fitch[c], S.N. Konchenko[a,b]

[a] *Nikolaev Institute of Inorganic Chemistry, Siberian Branch, Russian Academy of Sciences, 630090 Novosibirsk, Russia.*

[b] *Department of Natural Sciences, National Research University – Novosibirsk State University, 630090 Novosibirsk, Russia*

[c] *European Synchrotron Radiation Faculty, B.P. 220, Grenoble CEDEX, France*

** Email address sukhikh@niic.nsc.ru*

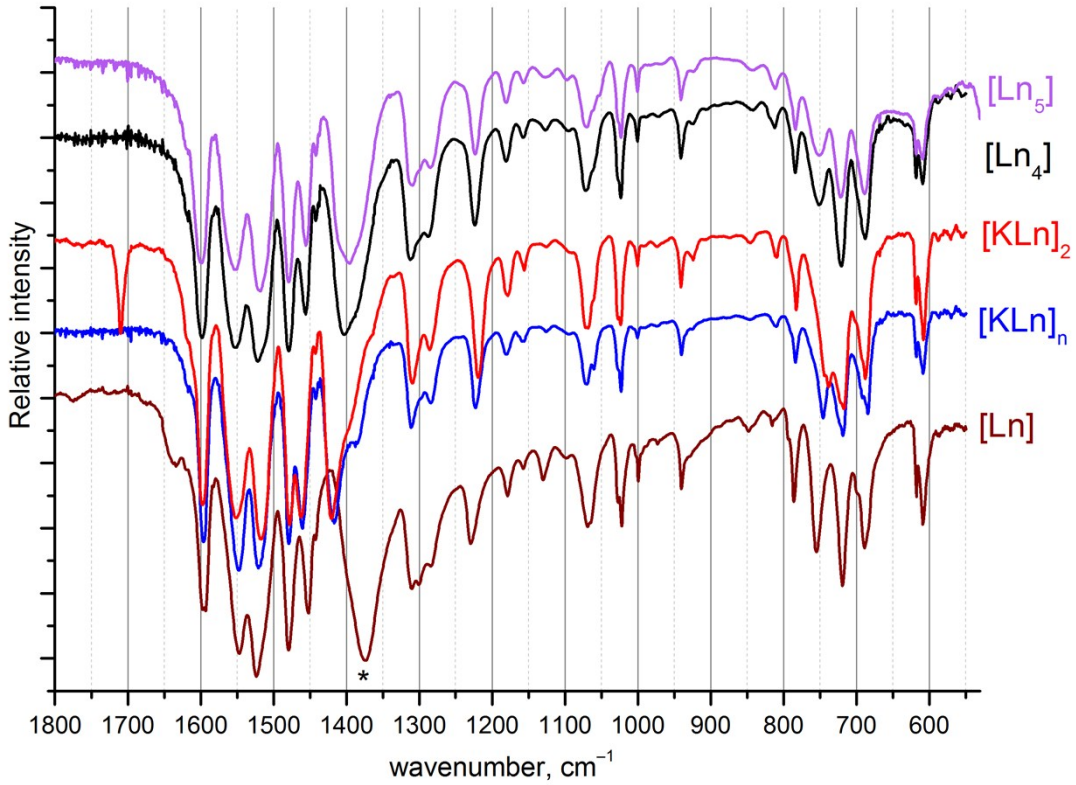

Fig. S1. Typical IR spectra of the complexes $[Ln_5(dbm)_{10}(OH)_5]$ (**[Ln$_5$]**) on the example of Ln = Sm; $[Ln_4(dbm)_{10}(OH)_2]$ (**[Ln$_4$]**), $[K(Me_2CO)Ln(dbm)_4]_2$ (**[KLn$_2$]**), $[KLn(dbm)_4]_n$ (**[KLn]$_n$**) and $[Ln(dbm)_3(H_2O)]$ (**[Ln]**) on the example of Ln = Eu. The most notable band difference is marked with asterisk. In the spectrum of $[K(Me_2CO)Ln(dbm)_4]_2$, the band at 1702 cm^{-1} corresponds to coordinated acetone.

Table S1. Crystallographic data of the complexes. Due to poor data quality for $[Nd_3(dbm)_8(OH)(H_2O)]\cdot 3.5C_7H_8$ and $[K(Me_2CO)Eu(dbm)_4]_2$, only the unit cell parameters are listed.

Compound	$[Dy(dbm)_3(H_2O)]$	$[KYb(dbm)_4]_n \cdot 2nCH_2Cl_2$	$[KEu(dbm)_4]_n \cdot 2nCH_2Cl_2$	$[KEu(dbm)_3(OBz)]_n$	$[K(Me_2CO)Dy(dbm)_4]_2$	$[K(Me_2CO)Eu(dbm)_4]_2$	$[Nd_3(dbm)_8(OH)(H_2O)] \cdot 3.5C_7H_8$	$[Nd_4(dbm)_{10}(OH)_2] \cdot C_7H_8$	$[Sm_5(dbm)_{10}(OH)_5] \cdot 3.5CH_2Cl_2$
Empirical formula	$C_{45}H_{35}DyO_7$	$C_{62}H_{48}Cl_4KO_8Yb$	$C_{62}H_{48}Cl_4EuKO_8$	$C_{52}H_{38}EuKO_8$	$C_{126}H_{100}Dy_2K_2O_{18}$	$C_{126}H_{100}Eu_2K_2O_{18}$	$C_{144.5}H_{116}Nd_3O_{18}$	$C_{157}H_{120}Nd_4O_{22}$	$C_{153.5}H_{122}Cl_7O_{25}Sm_5$
Formula weight	850.23	1274.94	1253.86	981.88	2305.25	2284.17	2573.09	2935.47	3366.40
Temperature/K	298(2)	150(2)	150(2)	150(2)	150(2)	150(2)	100(2)	150(2)	150(2)
Space group	*R3*	*C2/c*	*C2/c*	$P2_1/c$	*C2/c*	*C2/c*	*P*-1	*P*-1	$P2_1/c$
a/Å	22.7056(10)	28.0739(8)	27.8136(7)	13.6797(4)	28.8124(5)	28.829(3)	17.301(3)	15.0415(5)	22.1650(11)
b/Å	22.7056(10)	7.8185(2)	7.8790(2)	13.7983(3)	28.9292(5)	28.898(3)	18.304(3)	15.0538(6)	17.4192(6)
c/Å	6.3514(3)	25.6588(7)	25.9138(6)	23.4521(6)	26.2157(5)	26.326(2)	21.227(4)	16.1542(6)	36.6500(18)
α/°	90	90	90	90	90	90	68.498(4)	78.7490(10)	90
β/°	90	108.7876(8)	108.8290(10)	102.9380(10)	104.6080(10)	104.501(3)	77.063(4)	66.6210(10)	100.372(2)
γ/°	120	90	90	90	90	90	76.663(5)	74.1200(10)	90
Volume/$Å^3$	2835.7(3)	5331.9(3)	5374.9(2)	4314.36(19)	21144.9(7)	21234(3)	6013.0(19)	3213.8(2)	13919.2(11)
Z	3	4	4	4	8	8	2	1	4
ρ_{calc}g/cm^3	1.494	1.588	1.549	1.512	1.448			1.516	1.606
μ/mm^{-1}	2.028	2.090	1.501	1.607	1.551			1.661	2.282
F(000)	1281.0	2564.0	2536.0	1984.0	9360.0			1476.0	6688.0
2Θ range for data collection/°	6.216 to 51.618	3.064 to 59.58	3.094 to 55.178	3.448 to 57.586	2.028 to 57.524			3.022 to 54.39	2.992 to 51.364
Index ranges	$-27 \le h \le 27$, $-27 \le k \le 27$, $-5 \le l \le 7$	$-34 \le h \le 38$, $-10 \le k \le 10$, $-35 \le l \le 35$	$-27 \le h \le 36$, $-8 \le k \le 10$, $-33 \le l \le 33$	$-18 \le h \le 18$, $-12 \le k \le 18$, $-31 \le l \le 31$	$-37 \le h \le 38$, $-39 \le k \le 36$, $-35 \le l \le 35$			$-19 \le h \le 11$, $-19 \le k \le 19$, $-20 \le l \le 16$	$-26 \le h \le 27$, $-21 \le k \le 20$, $-44 \le l \le 44$
Reflections collected	5976	22144	17168	75372	136904			25267	107404
Independent reflections	2087 [R_{int} = 0.0354]	7506 [R_{int} = 0.0259]	6210 [R_{int} = 0.0229]	11216 [R_{int} = 0.0275]	27414 [R_{int} = 0.0394]			14199 [R_{int} = 0.0248]	26411 [R_{int} = 0.0496]
restraints/parameters	49/160	0/344	0/344	0/559	0/1341			145/832	1428/1861
Goodness-of-fit on F^2	1.058	1.086	1.047	1.053	1.033			1.027	1.159
Final R indexes [I>=2σ (I)]	R_1 = 0.0236, wR_2 = 0.0587	R_1 = 0.0303, wR_2 = 0.0717	R_1 = 0.0245, wR_2 = 0.0582	R_1 = 0.0199, wR_2 = 0.0460	R_1 = 0.0274, wR_2 = 0.0598			R_1 = 0.0446, wR_2 = 0.1057	R_1 = 0.0704, wR_2 = 0.1453
Final R indexes [all data]	R_1 = 0.0236, wR_2 = 0.0587	R_1 = 0.0405, wR_2 = 0.0759	R_1 = 0.0305, wR_2 = 0.0613	R_1 = 0.0240, wR_2 = 0.0483	R_1 = 0.0376, wR_2 = 0.0654			R_1 = 0.0720, wR_2 = 0.1224	R_1 = 0.1040, wR_2 = 0.1668
Largest diff. peak/hole / e $Å^{-3}$	0.55/-0.38	1.06/-1.17	0.93/-0.60	0.59/-0.49	1.30/-1.20			1.67/-1.19	3.41/-1.82

Table S2. Average Ln–O and K–O bond lengths with standard deviation in the complexes, Å. Chel. abbreviation is for chelate dbm^-, chel.-br. – for chelate-bridging, bis-chel.-br. – for bis-chelate-bridging ones.

Compound	$Ln–OH_x$*	Ln–O (chel.)	Ln–O (chel.-br.)	Ln–O (bis-chel.-br.)	K–O
$[Dy(dbm)_3(H_2O)]$	2.415(8)	2.30(1)	–	–	–
$[KYb(dbm)_4]_n·2nCH_2Cl_2$	–	2.32(3)	–	–	2.94(2)
$[KEu(dbm)_4]_n·2nCH_2Cl_2$	–	2.40(3)	–	–	2.91(1)
$[KEu(dbm)_3(OBz)]_n$	–	2.38(3)	–	–	2.76(6)
$[K(Me_2CO)Dy(dbm)_4]_2$	–	2.35(4)	–	–	2.66(9)
$[Nd_4(dbm)_{10}(OH)_2]·C_7H_8$	2.44(2)	2.37(2)	2.44(2)	2.54(3)	–
$[Sm_5(dbm)_{10}(OH)_5]·3.5CH_2Cl_2$	2.41(4) 2.63(7)**	2.35(2)	2.43(5)	–	–

* x = 1, 2

** the first distance is for μ_3-OH, the second one is for μ_4-OH.

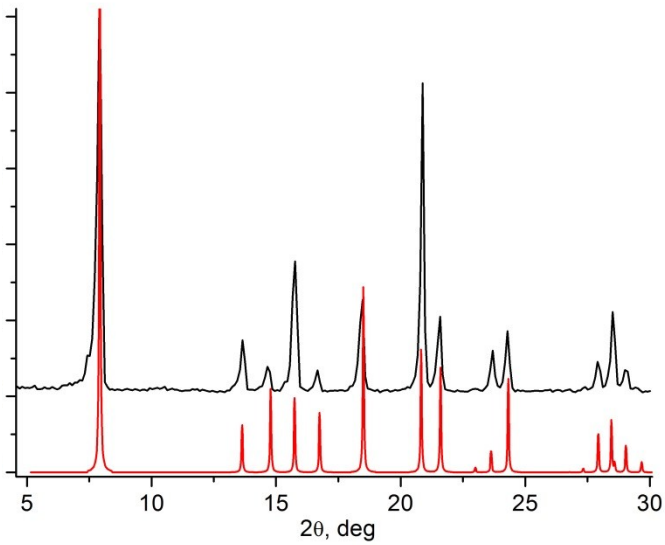

Fig. S2. Experimental (top) and simulated (bottom) powder XRD patterns for the complexes $[Ln(dbm)_3(H_2O)]$ on the example of Ln = Eu.

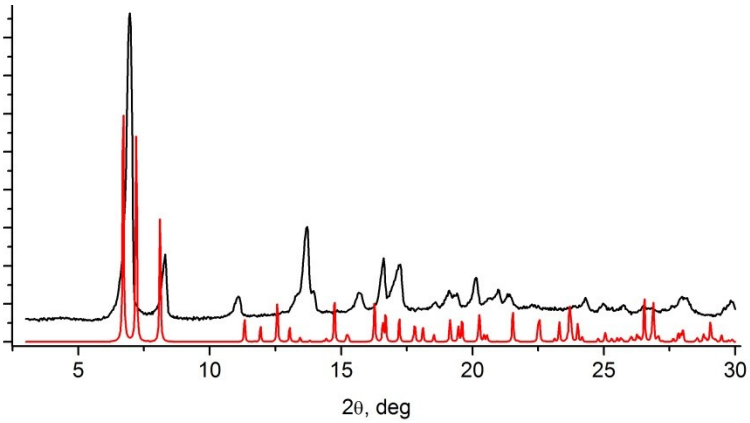

Fig. S3. Experimental (top) and simulated (bottom) powder XRD patterns for the complexes $[KLn(dbm)_4]_n$ on the example of Ln = Dy.

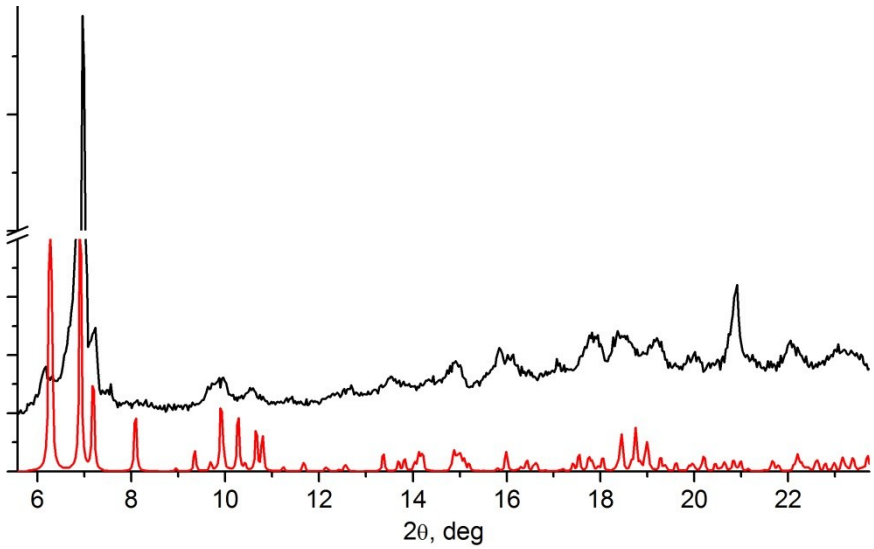

Fig. S4. Experimental (top) and simulated (bottom) powder XRD patterns for the complexes $[K(Me_2CO)Ln(dbm)_4]_2$ on the example of Ln = Dy.

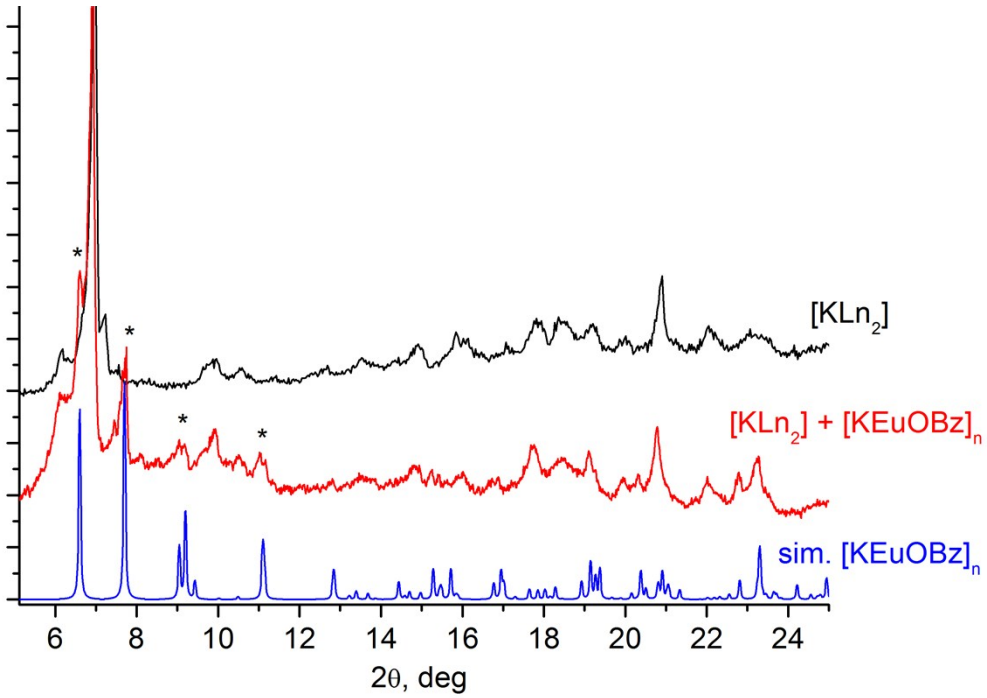

Fig. S5. Experimental powder XRD patterns for $[K(Me_2CO)Ln(dbm)_4]_2$ (**$[KLn_2]$**), the mixture of products $[K(Me_2CO)Ln(dbm)_4]_2$ and $[KEu(dbm)_3(OBz)]_n$ (**$[KLn_2]$ + [KEuOBz]**) and simulated one for $[KEu(dbm)_3(OBz)]_n$ (**[KEuOBz]**). The most notable peaks referred to $[KEu(dbm)_3(OBz)]_n$ marked with asterisk.

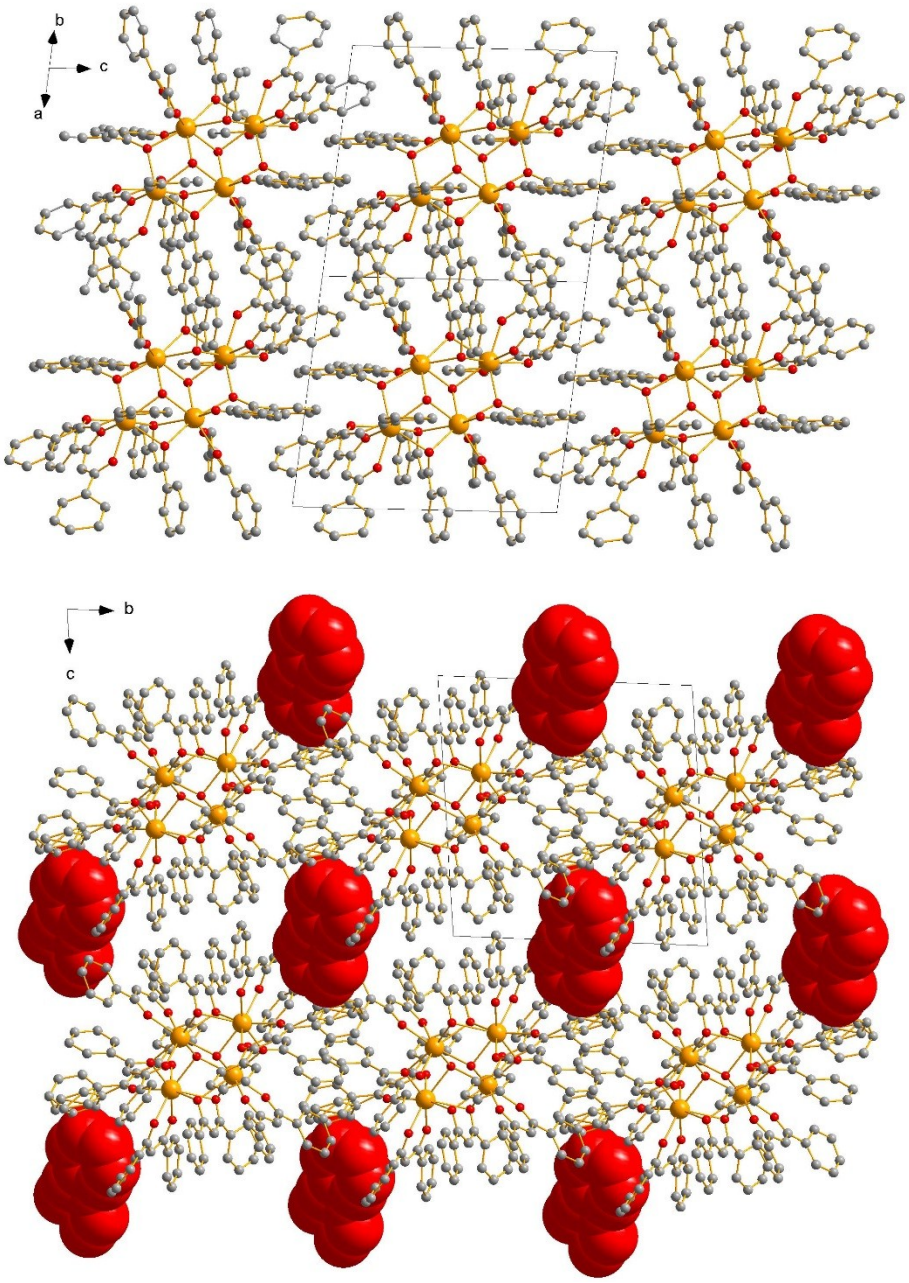

Fig. S6. Crystal packing of the complexes $[Nd_4(dbm)_{10}(OH)_2]$, top (V. Baskar, P.W. Roesky, Z. Anorg. Allg. Chem., 631 (2005) 2782-2785) and $[Nd_4(dbm)_{10}(OH)_2]\cdot C_7H_8$ obtained in this work, bottom. Solvate toluene molecules are shown in space-filling model (red).

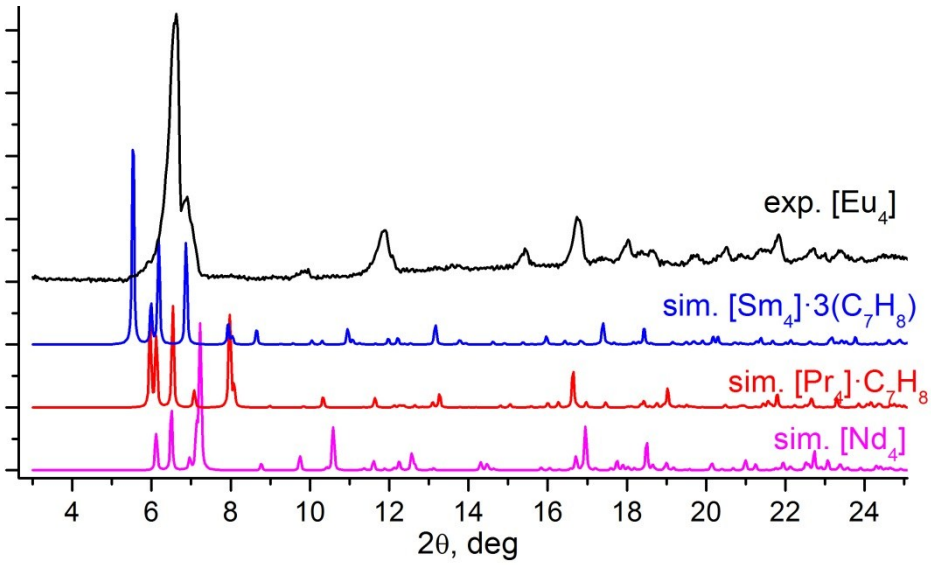

Fig. S7. Experimental and simulated powder XRD patterns for the complexes $[Ln_4(dbm)_{10}(OH)_2]$ on the example of Ln = Eu.

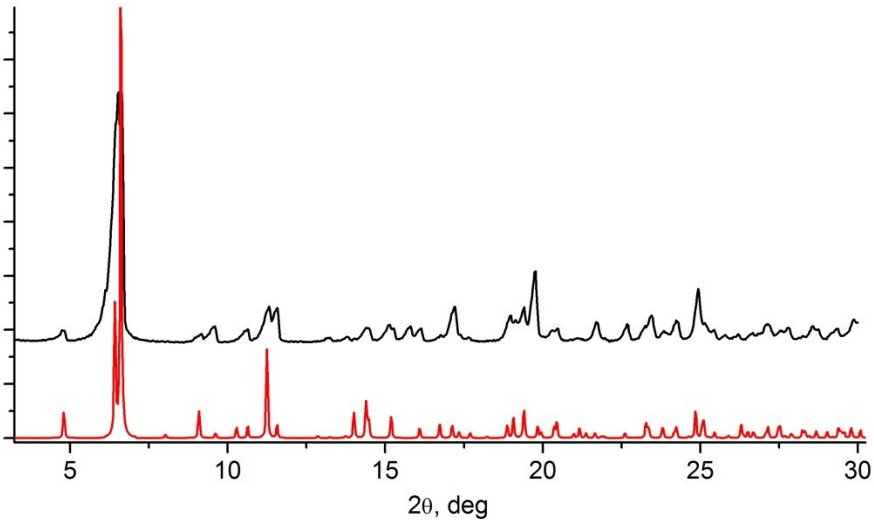

Fig. S8. Experimental (top) and simulated (bottom) powder XRD patterns for the complexes $[Ln_5(dbm)_{10}(OH)_5]$ (*P*4/*n* space group) on the example of Ln = Yb.

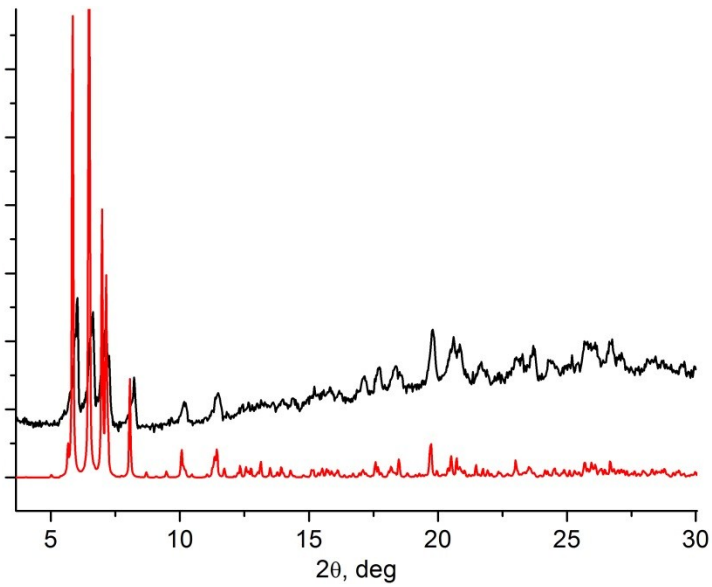

Fig. S9. Experimental (top) and simulated (bottom) powder XRD patterns for the complexes $[Ln_5(dbm)_{10}(OH)_5]$ ($P2_1/c$ space group) on the example of Ln = Sm.

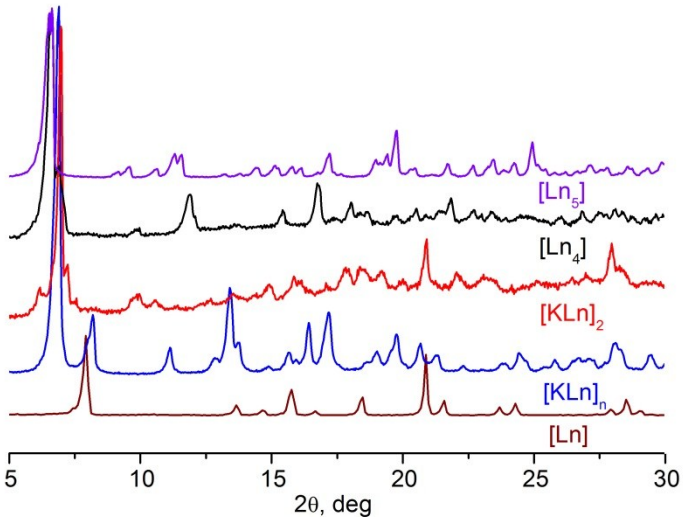

Fig. S10. Experimental powder XRD patterns for all of the types of the complexes, *viz*. $[Ln_5(dbm)_{10}(OH)_5]$ (**[Ln_5]**), $[Ln_4(dbm)_{10}(OH)_2]$ (**[Ln_4]**), $[K(Me_2CO)Ln(dbm)_4]_2$ (**[KLn_2]**), $[KLn(dbm)_4]_n$ (**[$KLn]_n$**) and $[Ln(dbm)_3(H_2O)]$ (**[Ln]**).

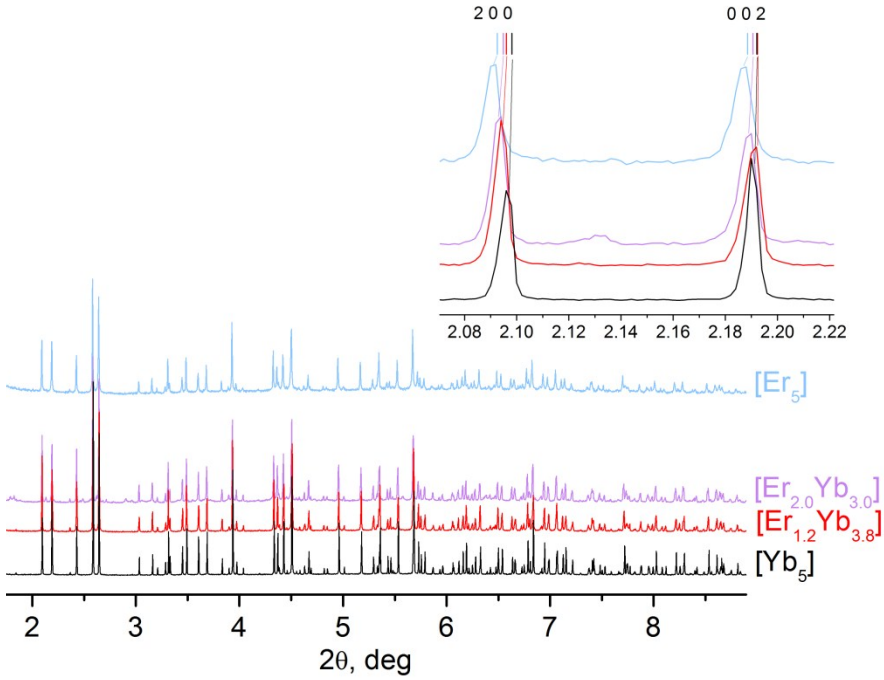

Fig. S11. High-resolution powder XRD patterns of the complexes $[Er_5(dbm)_{10}(OH)_5]$ (**Er_5**), $[Yb_5(dbm)_{10}(OH)_5]$ (**Yb_5**), $[Er_{1.2}Yb_{3.8}(dbm)_{10}(OH)_5]$ (**$Er_{1.2}Yb_{3.8}$**) and $[Er_{2.0}Yb_{3.0}(dbm)_{10}(OH)_5]$ (**$Er_{2.0}Yb_{3.0}$**). Detailed view of the peaks (2 0 0) and (0 0 2) is in the inset. Vertical lines show position of the reflections defined by Pawly method.

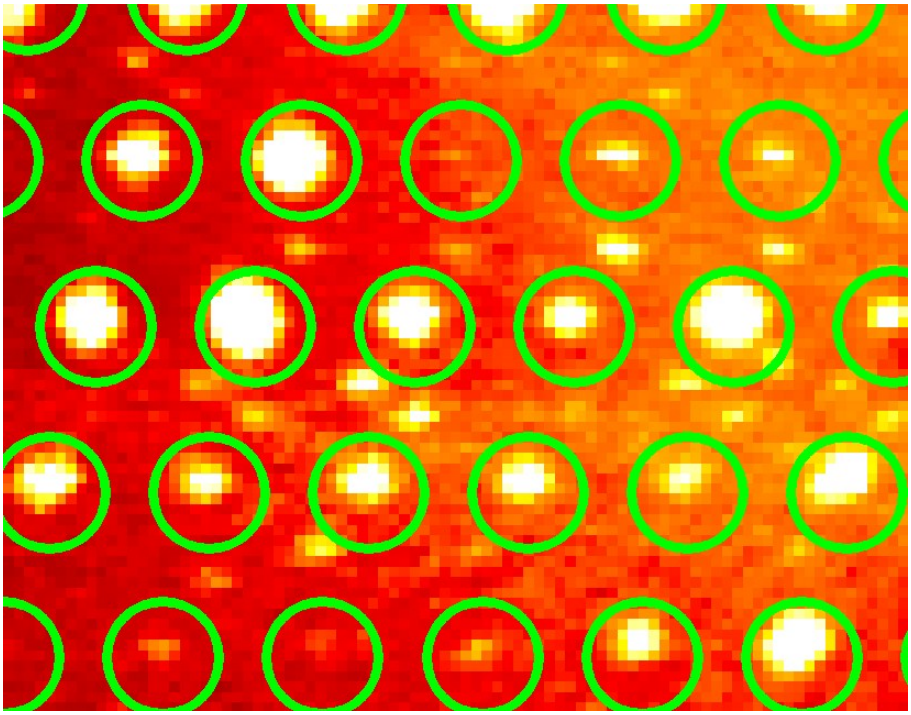

Fig. S12. Single-crystal diffraction pattern of the complex $[Nd_3(dbm)_8(OH)(H_2O)]\cdot 3C_7H_8$ in reciprocal space showing Bragg reflections (highlighted in green circles) and the satellites.